Unsupervised Brain Anomaly Detection in MR Images

Samuel Botter Martins*
Federal Institute of São Paulo, Brazil
University of Groningen, Netherlands
University of Campinas, Brazil

Alexandru Cristian Telea
Utrecht University, Netherlands

Alexandre Xavier Falcão
University of Campinas, Brazil

***Abstract*—Many brain anomalies are associated with abnormal asymmetries. To detect and/or segment such anomalies in brain images, most automatic methods rely on *supervised* learning. This requires a large number of high-quality annotated training images, which is lacking for most medical image analysis problems. In contrast, *unsupervised* methods aim to learn a model from unlabeled healthy images, so that an unseen image that breaks priors of this model, *i.e.,* an outlier, is considered an anomaly. This paper addresses the development of solutions to leverage *unsupervised* machine learning for the detection/analysis of abnormal brain asymmetries related to anomalies in magnetic resonance (MR) images. Experimental results on 3D MR-T1 images from healthy subjects and patients with a variety of lesions show the effectiveness and robustness of the proposed unsupervised approaches for brain anomaly detection.**

I. Introduction

Deviations from the *normal* pattern of brain asymmetries are useful insights about neurological pathologies [1]. Morphological changes in (sub)cortical in one or both hemispheres characterize these structural abnormalities, as shown in Fig. 1. Hence, to identify and detect many abnormalities in the brain, defining *normal* brain asymmetries is crucial.

To detect or segment brain anomalies, most automatic methods in the literature rely on supervised machine learning. Such methods commonly have three main limitations: (i) They require a large number of annotated training images, which is absent for most medical image analysis problems [2]–[4]; (ii) They are only designed for the lesions found in the training set, so generalization is challenging; (iii) Some methods still require weight fine-tuning (retraining) when used for a new set of images due to image variability across scanners and acquisition protocols, limiting their application in clinical routine.

All the above limitations of supervised methods motivate research on *unsupervised* anomaly detection approaches [5]–[11]. From a training set with images of *healthy* subjects *only*, these methods encode general knowledge or assumptions (*priors*) from healthy tissues, so that outliers who break such general priors are considered anomalous [7]. Unsupervised detection methods do not use labeled samples, so they are less effective in detecting lesions from a specific condition than supervised approaches trained from labeled samples for that condition. For the same reason, however, unsupervised methods are generic in detecting *any* lesions, *e.g.,* coming from multiple conditions, as long as these notably differ from healthy training samples.

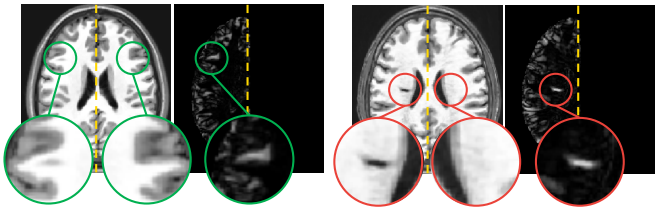

(a) (b)

Fig. 1: MR images and their corresponding asymmetry maps for (a) a healthy subject and (b) a stroke patient. Green borders indicate pairs of regions with normal asymmetries. Red borders indicate abnormal asymmetries resulted from a stroke. Normal asymmetries are accentuated on the brain cortex. Both cases omit other regions with normal asymmetries.

Combining the pros and cons of unsupervised methods listed above, as well as the importance of identifying abnormal brain asymmetries associated to brain anomalies, this paper summarizes the solutions proposed in the Ph.D. thesis [12] to answer the following key research questions:

RQ1: *Can we model normal brain asymmetries?*
RQ2: *Can we use the normal brain asymmetry model to detect brain anomalies?*

To illustrate how we approach answering these questions, we consider the typical pipeline for brain image processing and analysis (Fig. 2). Given a 3D MR-T1 image, we first perform several preprocessing tasks (*e.g.,* noise filtering and intensity normalization) to overcome inherent acquisition issues, such as noise and inhomogeneity fields. Next, we define the *volumes of interest* (VOIs) to be analyzed: either the entire brain or some specific region. Features related to brain asymmetries are extracted from these VOIs and subsequently classified as *normal* or *abnormal* from the knowledge about normal asymmetries present in a training set of control images. We evaluate our approaches on 3D MR-T1 images, mainly due to the larger availability of public datasets of healthy and

* This paper is related to the thesis of Samuel Botter Martins resulting from a joint Ph.D. program between the University of Campinas (Brazil) and University of Groningen (Netherlands).

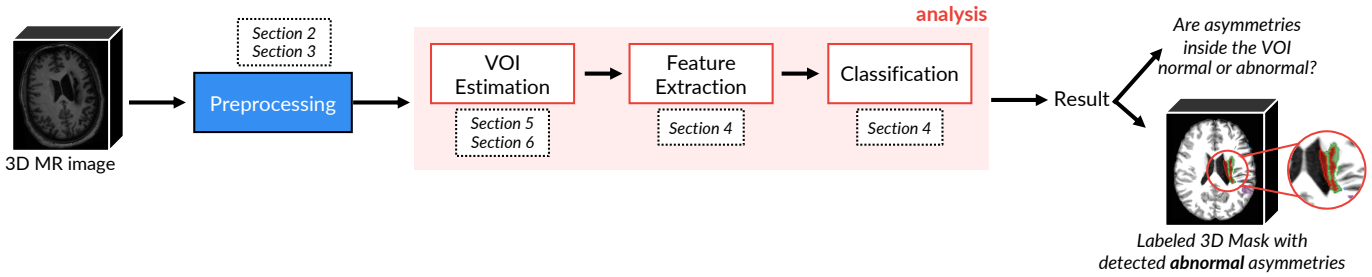

Fig. 2: General pipeline considered in the thesis to explore novel unsupervised brain anomaly detection approaches.

abnormal brain volumetric images for this imaging modality.

The remainder of the paper describes the steps of the pipeline in Fig. 2 in a bottom-up way as follows. Section II reviews the typical MRI preprocessing operations considered in this work. Section III summarizes our solution for brain image segmentation to define our target macro-regions of interest. Section IV proposes an automatic method for the detection of abnormal hippocampi from abnormal asymmetries. Section V presents a more generic solution to detect abnormal asymmetries in the entire brain hemispheres. Section VI extends this last step to detect lesions (symmetric or asymmetric) in the hemispheres, cerebellum, and brainstem. Finally, Section VII presents a compilation of our contributions and experimental findings, along with future research perspectives.

II. MRI Preprocessing

Automatic analysis of MR images is challenging due to typical acquisition artifacts — *e.g.,* noise, inhomogeneities, and variability of intensity and contrast — which negatively impact both medical diagnosis and automatic analysis. We use typical MRI preprocessing steps to reduce these artifacts and, consequently, improve the image quality for subsequent analysis, as shown in Fig. 3.

For each 3D image (Fig. 3a), we start performing noise reduction by median filtering, followed by MSP alignment, and bias field correction by N4 [13]. As voxels from irrelevant tissues/organs for the addressed problem (*e.g.,* neck and bones) can negatively impact the image registration and intensity normalization, we use AdaPro (Section III) to automatically segment the *macro regions of interest*: right and left hemispheres, cerebellum, and brainstem (Fig. 3b).

To attenuate differences in brightness and contrast among images, we apply a *histogram matching* (of image intensities) between the segmented images and the template, considering only the voxels inside the regions of interest (Fig. 3d). We then perform deformable registration to place all images in the coordinate space of the MNI template [14]. Finally, we perform another histogram matching between the registered images and the template (Fig. 3e).

III. Automatic Brain Image Segmentation

Automated segmentation of brain structures (*e.g.,* organs and lesions) in 3D MR brain images for quantitative analysis has been a challenge and Probabilistic Atlases (PAs) are among the most successful approaches [15], [16]. However, the existing models do not adapt to possible object anomalies due to the presence of a condition or a surgical procedure.

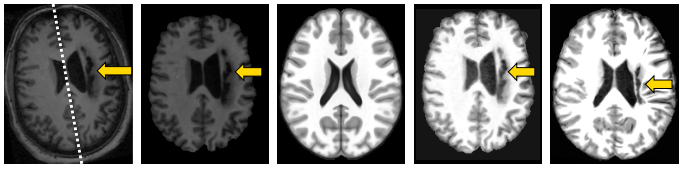

Fig. 3: 3D MR image preprocessing. **(a)** Axial slice of a raw stroke (pointed by arrow) 3D image. **(b)** Test image after noise filtering, MSP alignment, bias field correction, and brain segmentation. **(c)** Symmetric reference image. **(d)** Histogram matching between (b) and (c). **(e)** Final preprocessed image.

To address the above limitation, we present an effective and efficient adaptive probabilistic atlas, named *AdaPro* [17]. Our method incorporates a texture classifier during object delineation to adapt shape constraints on-the-fly according to the presence of detected anomalies in the target image. Fig. 4 shows resulting images of AdaPro's steps for the segmentation of both hemispheres and cerebellum for an anomalous image.

Regarding our research questions, brain segmentation supports our proposed unsupervised anomaly detection at different steps: (i) for intensity normalization (Section II); (ii) to warp both hemispheres for anomaly detection on the native image space (Section V); and (iii) to perform anomaly detection in each object of interest individually (Section VI).

A. Atlas Construction

Let a training set $X = \{A_1, \ldots, A_n\}$ with n atlases of healthy subjects, where each *atlas* $A_i = (I_i, M_i)$ consists of a source 3D image I_i and its corresponding label image M_i with the mask of each 3D object of interest. Let $A_r = (I_r, M_r)$ be the standard reference coordinate space (*template*) – AdaPro's pipeline only uses I_r.

For each object of interest m, we build a *probabilistic atlas* P_m by counting the frequency of the label assignment from all training registered atlases $A_i \in X$ and keeping the most-often assigned label to each voxel. This frequency gives the *prior* probability of the voxel to belong to object m. All voxels with probability 1 form the *certainty region* whereas those

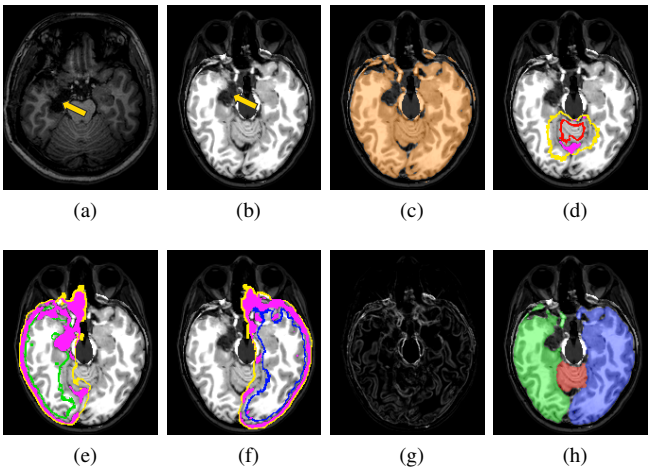

Fig. 4: AdaPro segmentation. **(a)** Axial slice of an input post-surgery 3D MR-T1 image (the arrow indicates an anomaly). **(b)** Preprocessed input image. **(c)** Positive voxels (orange) after texture classification. **(d)–(f)** Estimated seeds from the adaptive models for the background and target objects. Magenta voxels indicate the forbidden regions imposed by (c). **(g)** Gradient of (b). **(h)** Delineated objects in 2D (axial slice).

within (0, 1) form the *uncertainty region*, where the object's boundaries are likely to fall.

We then design a binary classifier C based on a linear Support Vector Machine [18] by interactively selecting training voxels on the 3D template I_r. Brain tissue voxels are considered positive samples; voxels with typically different intensities, *e.g.*, cerebrospinal fluid (CSF) and image background, are the negative samples. Each training voxel is represented by its intensity and the intensities of all neighbors inside a sphere of radius 5.0 voxels, resulting in a 515-dimensional feature vector.

B. Image Segmentation

Let I_t represent a target 3D brain image after the preprocessing in Section II (Fig. 4b). We aim to estimate a seed set $\mathcal{S} = \mathcal{S}_0 \cup \mathcal{S}_m$, where $\mathcal{S}_m$, $m > 0$, contains seed voxels selected inside object m, and $\mathcal{S}_0$ contains seed voxels selected in the background. The borders of the dilated and eroded certainty region of P_m form S_0 and S_m, respectively. The dilation and erosion slightly increase the uncertain region of P_m. To identify regions on I_t where shape constraints should be adapted, AdaPro classifies I_t with the binary classifier C (Fig. 4c). Then, the complement of the classification forms a *forbidden region* F (magenta voxels in Figs. 4d–f) that eliminates its voxels from the competition between internal and external seeds during object delineation.

For the delineation of each object m, AdaPro uses the Relaxed Image Foresting Transform (RIFT) algorithm [19]. RIFT first computes a watershed transform from labeled seeds defined by $\mathcal{S} = \mathcal{S}_0 \cup \mathcal{S}_m$. The seed competition takes into account the gradient image of I_t (Fig. 4g) and outputs the final object segmentation (Figs. 4h) that does not include anomalies (arrow in Fig. 4b).

C. Experiments and Results

We conducted a set of experiments on six in-house datasets of 3D MR-T1 brain images of healthy subjects and patients with epilepsy. We compared AdaPro to segment the cerebellum (C), right hemisphere (RH), and left hemisphere (LH) against three state-of-the-art atlas-based methods: SOSM-S [15], volBrain [20], and a MALF technique [21].

Table I shows the Average Symmetric Surface Distance (ASSD) for the two datasets of epileptic patients before (PRE-3T) and after lobe resection (POST-3T). The numbers correspond to the mean and standard deviation values of all instances of each object.

AdaPro is more accurate than the baselines in both datasets for all objects of interest, especially for post-surgery images. These results are consistent in the other datasets but, due to lack of space, their results were omitted in this paper. We refer to [12], [17] for the complete and detailed experiments.

TABLE I: Comparison of ASSD (mm) for the Cerebellum (C), Right Hemisphere (RH), and Left Hemisphere (LH) of the pre- and post-operative images of **3T**. Lower ASSD means better accuracy (bold scores are the best with statistical significance).

		SOSM-S	MALF	volBrain	AdaPro
PRE-3T	C	0.91 ± 0.22	1.02 ± 0.31	1.02 ± 0.08	**0.75 ± 0.07**
	RH	1.04 ± 0.14	1.07 ± 0.18	1.42 ± 0.11	**1.03 ± 0.18**
	LH	1.02 ± 0.13	1.06 ± 0.17	1.36 ± 0.10	**1.01 ± 0.14**
POST-3T	C	0.90 ± 0.19	1.00 ± 0.28	1.01 ± 0.09	**0.75 ± 0.09**
	RH	1.28 ± 0.20	1.30 ± 0.16	1.51 ± 0.14	**1.08 ± 0.18**
	LH	1.25 ± 0.18	1.25 ± 0.20	1.47 ± 0.13	**1.10 ± 0.18**

IV. Detection of Abnormal Hippocampal Asymmetries

We next present our first unsupervised solution for our research questions. We propose (i) an unsupervised framework to model *normal* brain asymmetries from healthy subjects and (ii) use this model to detect abnormal asymmetries. Our solution does not need the segmentation of the target structures or data annotation. We prove our solution for the detection of abnormal hippocampal asymmetries from epilepsy patients (Fig. 5).

We start creating VOIs around structures of interest. These VOIs can be defined as 3D bounding boxes from segmentation, whenever they are available. For VOI creation in new images, we propose a fast and accurate *3D patch-based model*. We refer to [12], [22] for details.

Next, a *generative deep neural network* — a *convolutional autoencoder* (CAE) [23] — is used to learn the image transformation from the left VOI to the flipped right VOI and vice-versa. Fig. 6 shows the considered architecture used for normal *hippocampal asymmetry* representation. We concatenate the outputs of the intermediate layers from the CAE to form each sample (feature vector) of a *normal* structural asymmetry.

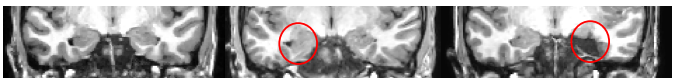

(a) (b) (c)

Fig. 5: Cropped coronal slices that show: (a) normal hippocampal asymmetries, (b) left hippocampal atrophy, and (c) postoperative hippocampus.

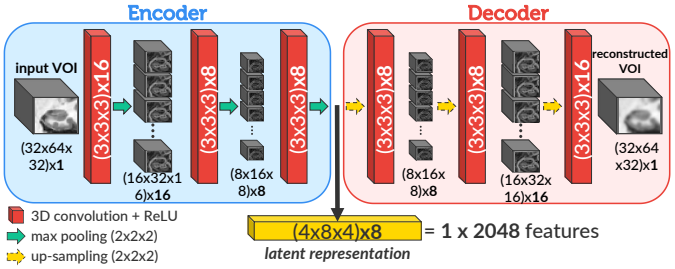

Fig. 6: Architecture of the convolution autoencoder (CAE) used for normal VOI asymmetry representation.

Finally, we train a *one-class classifier* (OCC) that corresponds to our *normal* brain asymmetry model, thus addressing our research question **RQ1**. For this, we initial consider the popular One-Class SVM [24]. Then, we propose a novel OCC, called OC-OPF, based on the Optimum Path Forest algorithm [25] — we evaluate both classifiers in the next section. We use the OCC to detect outliers as abnormal brain asymmetries, which addresses **RQ2**.

A. Experiments and Results

We considered 575 3D MR-T1 brain images from healthy subjects (CONTROLS), and epilepsy patients which are divided into four datasets: (PRE) preoperative patients with unilateral hippocampal atrophy (47 images); (POST) postoperative patients (88 images); (RHA) patients with right hippocampal atrophy (34 images); and (LHA) patients with left hippocampal atrophy (37 images).

We combined the convolutional-autoencoder (CAE) representation (Fig. 6) with each one-class classifier, OC-SVM [24] and OC-OPF, which were trained in the *original feature space* and the *two-dimensional spaces* after non-linear projection by t-SNE [26], a popular projection algorithm widely used in several machine-learning problems. According to Rauber *et al.* [27], the separation among groups (classes) in the 2D projection space, as created by the t-SNE, is a strong indication of their separation in the original feature space.

Table II presents the average detection scores in the *original* and *projection feature space* for hippocampal asymmetries. These scores show the percentage of the classification hits of controls images as normal hippocampal asymmetries and patient images as abnormal hippocampal asymmetries.

The combination CAE/OC-SVM provides slightly better accuracies than CAE/OC-OPF in most datasets in the original space, with no errors for PRE and POST. The use of the projection space has a surprisingly positive impact on the

TABLE II: Anomaly detection scores (%) in the original and projection feature space for the proposed framework.

	Original Feature Space		**Projection Space by t-SNE**	
	OC-SVM	OC-OPF	OC-SVM	OC-OPF
CONTROLS	86.61 ± 2.30	89.04 ± 2.55	96.22 ± 2.72	**99.72 ± 0.18**
PRE	**100.0 ± 0.00**	98.40 ± 2.04	**100.0 ± 0.00**	**100.0 ± 0.00**
POST	**100.0 ± 0.00**	**100.0 ± 0.00**	**100.0 ± 0.00**	**100.0 ± 0.00**
RHA	99.26 ± 1.47	97.06 ± 4.16	**100.0 ± 0.00**	**100.0 ± 0.00**
LHA	99.32 ± 1.35	97.30 ± 5.41	**100.0 ± 0.00**	**100.0 ± 0.00**

results: the best detection scores for control images have considerably increased (from 89.04% to 99.72%), and there are no classification errors for patient images in both classifiers.

Finally, to better understand these results, Fig. 7 presents a t-SNE projection space. Each point shows hippocampal asymmetries of a given pair of hippocampi (VOI) as extracted by CAE. By clicking on any point on the plot, the user can see the corresponding slice across the centers of the VOIs. It is also possible to navigate in the image around that location for inspection and annotation of the anomaly type.

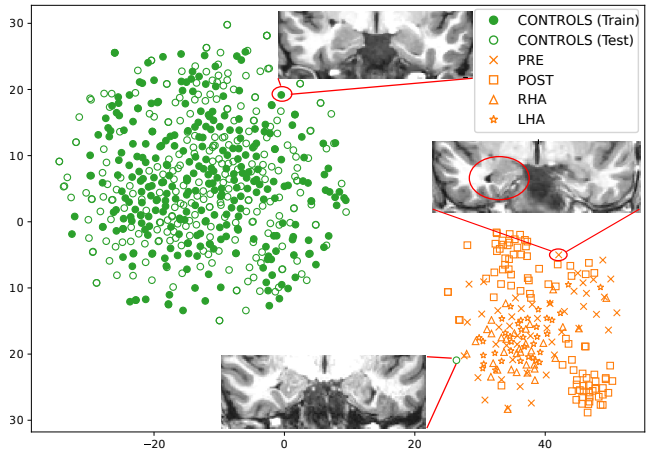

Fig. 7: The 2D t-SNE projection from the considered datasets for the CAE-based representations. The expert can select any observation from the projection to inspect its image slices (see cropped slices of selected observations).

We have extended this unsupervised abnormal hippocampal asymmetry detection for the entire hemispheres. From a set of pairs of VOIs automatically extracted in the hemispheres by uniform grid-sampling, we performed our proposed solution for each pair. As detailed in [12], experiments show poor results with several false-positive asymmetries detected for all considered images, mainly for using 3D patches. This limitation motivated us to use *supervoxel segmentation* to estimate VOIs for brain asymmetry detection, as detailed in the next section.

V. Detection of Abnormal Brain Asymmetries

This section proposes an automatic unsupervised framework, called *Supervoxel-based Abnormal Asymmetry Detec-*

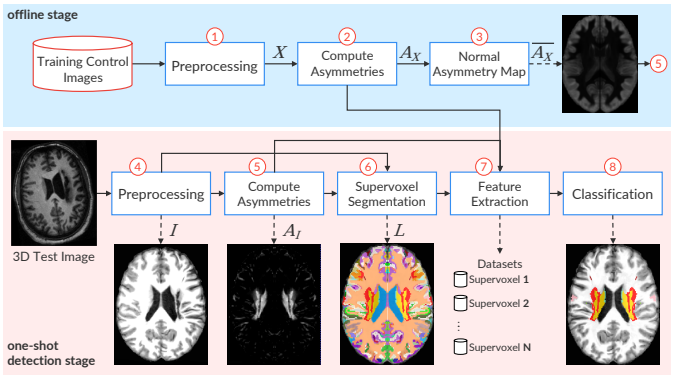

Fig. 8: The pipeline of SAAD. Steps 1 to 3 (blue part) are performed offline. Steps 4 to 8 (pink part) are computed for each 3D test image (detection stage). The output images from Steps 3, 5, 6, and 8 are visualized as a symmetrical image. However, the method can consider just one hemisphere.

tion (SAAD) [9], [10], [28], for detecting abnormal asymmetries associated with anomalies in 3D MR brain images. Fig. 8 presents the pipeline of SAAD. We next discuss the eight steps of this pipeline.

A. Asymmetry Computation

Let X be the set of registered training 3D images (output of Step 1) and I the test 3D image after preprocessing (output of Step 4). We obtain the set of asymmetry maps A_X for all X by computing the voxel-wise absolute differences between left and right hemispheres (Step 2). Next, we create a *normal asymmetry map* $\overline{A_X}$ (Step 3) by averaging the absolute difference values over all A_X (Step 3). We use this map to reduce the detection of false-positive asymmetries in I in commonly asymmetric brain regions (*e.g.,* cortex). Finally, we compute voxel-wise absolute differences between the hemispheres for I and then subtract $\overline{A_X}$ from them. Resulting positive values form a final asymmetry map A_I for the test image I (Step 5).

B. Symmetric Supervoxel Segmentation

We propose a new method, named *SymmISF*, that extracts symmetrical supervoxels from left and right brain hemispheres simultaneously (output of Step 6). SymmISF is based on the recent *Iterative Spanning Forest* (ISF) framework [29] for superpixel segmentation and has three steps: (i) seed sampling followed by multiple iterations of (ii) connected supervoxel delineation, and (iii) seed recomputation to improve delineation. We refer to [12], [28] for more details of different strategies for each of these steps.

C. Feature Extraction and Classification

For each 3D test image I, each pair of symmetrical supervoxels is used to create a *specialized* one-class classifier (OCC) using as feature vector the normalized histogram of the asymmetry values inside the pair (Step 7). Classifiers are trained from control images only, thus locally modeling normal asymmetries for the entire hemispheres. Finally, SAAD uses the trained OCCs to find supervoxels with abnormal asymmetries in the corresponding testing image (Step 8).

SAAD can be also used to detect abnormal asymmetries in the native image space. For space reasons, we do not discuss this extension, but refer the interested reader to [10], [12].

D. Experiments and Results

We next summarize some experimental results from our method and the baselines extracted from [12], [28]. We refer to these works for a more deep evaluation for SAAD, including more baselines and metrics.

Datasets: For training, we considered the CamCan dataset [30], which has 653 3D MR-T1 images of 3T from healthy subjects. We visually inspected all MR-T1 images and removed images with bad acquisition or artifacts, yielding 524 images. For testing, we evaluated our approach on 3D MR-T1 images of the ATLAS dataset [31], which contains manually annotated lesions in images of stroke patients.

Baselines: We compared SAAD against the convolutional-autoencoder-based approach (CAE) from Chen *et al.* [6], which is, as far as we know, the current state-of-the-art *unsupervised* method for the ATLAS dataset. The method detects anomalies by thresholding the difference image between the input image and its reconstruction to obtain a binary segmentation, similarly to [5], [6]. We followed Baur *et al.* [5] and selected thresholds at the 85^{th} (CAE-85), and 90^{th} (CAE-90), and 95^{th} percentile from the histogram of reconstruction errors on the considered training set.

Metrics: Although SAAD detects abnormal asymmetries regardless of the type of anomalies, we can compute quantitative scores only for those lesions that are labeled in ATLAS, which are a subset of what SAAD can detect. For these lesions, we first computed the *detection rate* based on at least 15% overlap between lesions labeled in ATLAS with detected volumes of interest (VOIs) with abnormal asymmetries, as detected by SAAD (supervoxels) and CAE (segmented regions). Although our focus is on *detecting* abnormal asymmetries, we also measured the *Dice score* between lesions and the detected VOIs to check SAAD's potential as a *segmentation method*. Finally, we computed the relative *number of false-positive (FP) voxels* with respect to all classified voxels, *i.e.,* the total number of voxels inside the right hemisphere for SAAD, and both hemispheres for CAE.

Table III shows the mean results of SAAD against the baselines. CAE-85 and CAE-90 present considerably higher detection scores, 0.995 and 0.943, respectively, than SAAD (0.86). However, these impressive results are misleading as CAE reports drastically more false-positive voxels than SAAD (Table III, row 3). These high FP rates explain the poor Dice scores for CAE in Table III, which in turn are compatible with the ones reported in [6].

CAE yields very noisy detected regions that hinder the subsequent visual inspection while SAAD consistently detects well-defined abnormal asymmetries (see the images in

TABLE III: Comparison between SAAD and the baselines for the ATLAS dataset. Each result contains a box (inset) surrounding the lesion whose border color indicates if the lesion was detected (green) or missed (red).

		CAE-85	CAE-90	SAAD
1	Detection rate	**0.995 ± 0.002**	0.943 ± 0.018	0.862 ± 0.013
2	Dice	0.018 ± 0.003	0.017 ± 0.003	**0.19 ± 0.018**
3	FP voxel rate	0.4 ± 0.002	0.267 ± 0.001	**0.014 ± 0.002**

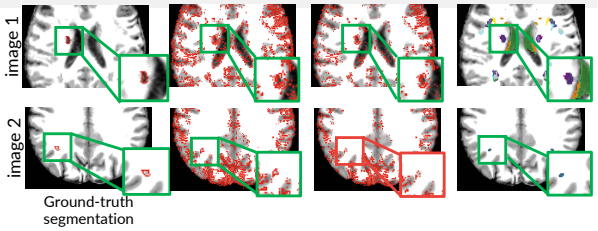

Table III). SAAD can also find small abnormal asymmetries (Table III), obtaining higher detection scores and considerably lower false-positive rates compared to the baselines. However, its analysis is limited to asymmetric anomalies in the *brain hemispheres* (for only relying on brain asymmetries), ignoring lesions in the cerebellum and brainstem. Also, it cannot detect similar and "symmetric" anomalies located roughly in the same region in both hemispheres, because of lack of accentuated asymmetries. These limitations are addressed in the next section.

VI. Detection of General Brain Anomalies

Our last contribution is to generalize SAAD by simply replacing asymmetry maps with any other distinct *saliency map*, which indicates what is important to analyze an image according to a specific problem – in our context, these are brain anomalies. This map extends the detection of (a)symmetric anomalies to the cerebellum and brainstem, thus overcoming SAAD's limitations (see Section V-D).

We instantiate this generic pipeline by considering *registration errors* for the saliency map. We assume that registration errors for *anomalies* are considerably different from errors for *healthy* tissues (Section 9). We call this method *Brain Anomaly Detection based on Registration Errors and Supervoxel Classification* (BADRESC) [8].

We adopted the same evaluation protocol presented in Section V-D. SAAD presents better detection rates (0.862) for hemispheric lesions compared to BADRESC (0.824). BADRESC reports a slightly worse Dice score (0.169) than SAAD (0.19) and similar false-positive voxel rates. However, BADRESC is able to detect anomalies in the cerebellum and brainstem with a promising detection rate (0.683). Fig. 9 presents some visual results. We refer to the works [8], [12] for more experiments and visual results.

VII. Conclusion

This paper addresses the development of solutions to leverage unsupervised machine learning for the detection/analysis

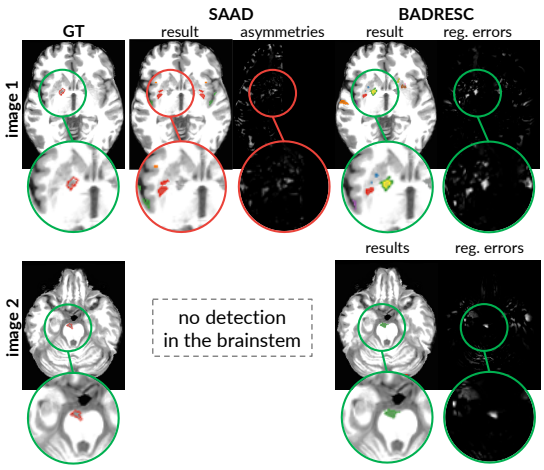

Fig. 9: Comparison between SAAD and BADRESC for stroke images. We show a slice of the result and corresponding saliency map for both methods. Each image contains an inset surrounding the lesion whose border color indicates if the lesion was detected (green) or missed (red).

of abnormal brain asymmetries related to anomalies in magnetic resonance (MR) images. We first proposed a robust automatic probabilistic-atlas-based approach for anomalous brain image segmentation. Second, we explored an automatic method for the detection of abnormal hippocampi from abnormal asymmetries based on convolutional autoencoders and one-class classifiers (OCCs). Third, we presented a more generic framework to detect abnormal asymmetries in the entire brain hemispheres using symmetrical supervoxels and OCCs. Finally, we generalize the previous solution for the detection of (a)symmetric lesions based on registration errors. Experimental results on 3D MR-T1 images from healthy subjects and patients with a variety of lesions show the effectiveness and robustness of the proposed unsupervised approaches for brain anomaly detection.

For future work, we suggest further investigating the impact of the t-SNE projection in the design of classifiers and extend the autoencoder-based framework to other well-defined brain structures. For the supervoxel-based framework, one could focus on designing saliency maps for a given specific problem — *e.g.,* a map that only highlights tumors — so that detection and segmentation scores will be maximized for such a problem. One can also explore other feature-extraction techniques, since we only considered a simple normalized histogram for that.

Acknowledgment

The authors thank CNPq (303808/2018-7), and FAPESP (2014/12236-1) for the financial support.

Publications

The thesis is the result of the following publications (in chronological order): [32], [33] **(honorable mention)**, [9], [10], [17], [22], [28], [8] **(best student paper)**, [34].

Other publications during the development of the thesis include: [35]–[39].

REFERENCES

[1] A. A. Woolard and S. Heckers, "Anatomical and functional correlates of human hippocampal volume asymmetry," *Psychiatry Research: Neuroimaging*, vol. 201, no. 1, pp. 48–53, 2012.

[2] Z. Akkus and et al., "Deep learning for brain MRI segmentation: state of the art and future directions," *Journal of Digital Imaging*, vol. 30, no. 4, pp. 449–459, 2017.

[3] M. Havaei, A. Davy, D. Warde-Farley, A. Biard, A. Courville, Y. Bengio, C. Pal, P.-M. Jodoin, and H. Larochelle, "Brain tumor segmentation with deep neural networks," *Medical Image Analysis*, vol. 35, pp. 18–31, 2017.

[4] B. Thyreau, K. Sato, H. Fukuda, and Y. Taki, "Segmentation of the hippocampus by transferring algorithmic knowledge for large cohort processing," *Medical Image Analysis*, vol. 43, pp. 214–228, 2018.

[5] C. Baur, B. Wiestler, S. Albarqouni, and N. Navab, "Deep autoencoding models for unsupervised anomaly segmentation in brain MR images," in *International MICCAI Brainlesion Workshop*, 2018, pp. 161–169.

[6] X. Chen, N. Pawlowski, M. Rajchl, B. Glocker, and E. Konukoglu, "Deep generative models in the real-world: An open challenge from medical imaging," *arXiv preprint arXiv:1806.05452*, 2018.

[7] D. Guo, J. Fridriksson, P. Fillmore, C. Rorden, H. Yu, K. Zheng, and S. Wang, "Automated lesion detection on MRI scans using combined unsupervised and supervised methods," *BMC Medical Imaging*, vol. 15, no. 1, p. 50, 2015.

[8] S. B. Martins, A. X. Falcão, and A. C. Telea, "BADRESC: Brain anomaly detection based on registration errors and supervoxel classification," in *International Joint Conference on Biomedical Engineering Systems and Technologies: BIOIMAGING*, 2020, pp. 74–81, best student paper awards.

[9] S. B. Martins, G. Ruppert, F. Reis, C. L. Yasuda, and A. X. Falcão, "A supervoxel-based approach for unsupervised abnormal asymmetry detection in MR images of the brain," in *IEEE International Symposium on Biomedical Imaging (ISBI)*, 2019, pp. 882–885.

[10] S. B. Martins, A. C. Telea, and A. X. Falcão, "Extending supervoxel-based abnormal brain asymmetry detection to the native image space," in *IEEE Engineering in Medicine and Biology Society (EMBC)*, 2019, pp. 450–453.

[11] D. Sato, S. Hanaoka, Y. Nomura, T. Takenaga, S. Miki, T. Yoshikawa, N. Hayashi, and O. Abe, "A primitive study on unsupervised anomaly detection with an autoencoder in emergency head ct volumes," in *SPIE Medical Imaging*, 2018, p. 105751P.

[12] S. B. Martins, "Unsupervised brain anomaly detection in MR images," PhD thesis, University of Groningen, 2020.

[13] N. J. Tustison, B. B. Avants, P. A. Cook, Y. Zheng, A. Egan, P. A. Yushkevich, and J. C. Gee, "N4ITK: improved N3 bias correction," *IEEE Transaction on Medical Imaging*, vol. 29, no. 6, pp. 1310–1320, 2010.

[14] V. S. Fonov, A. C. Evans, R. C. McKinstry, C. R. Almli, and D. L. Collins, "Unbiased nonlinear average age-appropriate brain templates from birth to adulthood," *Neuroimage*, vol. 47, p. S102, 2009.

[15] R. Phellan, A. X. Falcão, and J. K. Udupa, "Medical image segmentation via atlases and fuzzy object models: Improving efficacy through optimum object search and fewer models," *Medical Physics*, vol. 43, no. 1, pp. 401–410, 2016.

[16] J. E. Iglesias and M. R. Sabuncu, "Multi-atlas segmentation of biomedical images: a survey," *Medical Image Analysis*, vol. 24, no. 1, pp. 205–219, 2015.

[17] S. B. Martins, J. Bragantini, C. L. Yasuda, and A. X. Falcão, "An adaptive probabilistic atlas for anomalous brain segmentation in MR images," *Medical Physics*, vol. 46, no. 11, pp. 4940–4950, 2019.

[18] C. Cortes and V. Vapnik, "Support-vector networks," *Machine Learning*, vol. 20, no. 3, pp. 273–297, 1995.

[19] F. Malmberg, I. Nyström, A. Mehnert, C. Engstrom, and E. Bengtsson, "Relaxed image foresting transforms for interactive volume image segmentation," in *SPIE Medical Imaging*, vol. 7623, 2010, p. 762340.

[20] J. V. Manjón and P. Coupé, "volBrain: An online MRI brain volumetry system," *Frontiers in Neuroinformatics*, vol. 10, 2016.

[21] S. K. Warfield, K. H. Zou, and W. M. Wells, "Simultaneous truth and performance level estimation (STAPLE): an algorithm for the validation of image segmentation," *IEEE Transaction on Medical Imaging*, vol. 23, no. 7, pp. 903–921, 2004.

[22] S. B. Martins, B. C. Benato, B. F. Silva, C. L. Yasuda, and A. X. Falcão, "Modeling normal brain asymmetry in MR images applied to anomaly detection without segmentation and data annotation," in *SPIE Medical Imaging*, vol. 10950, 2019, pp. 71–80.

[23] J. Masci, U. Meier, D. Cireşan, and J. Schmidhuber, "Stacked convolutional auto-encoders for hierarchical feature extraction," in *International Conference on Artificial Neural Networks*, 2011, pp. 52–59.

[24] L. M. Manevitz and M. Yousef, "One-class SVMs for document classification," *Journal of Machine Learning Research*, vol. 2, no. Dec, pp. 139–154, 2001.

[25] F. A. M. Cappabianco, A. X. Falcão, C. L. Yasuda, and J. K. Udupa, "Brain tissue MR-image segmentation via optimum-path forest clustering," *Computer Vision and Image Understanding*, vol. 116, no. 10, pp. 1047–1059, 2012.

[26] L. v. d. Maaten and G. Hinton, "Visualizing data using t-SNE," *Journal of Machine Learning Research*, vol. 9, pp. 2579–2605, Nov 2008.

[27] P. E. Rauber, A. X. Falcão, and A. C. Telea, "Projections as visual aids for classification system design," *Information Visualization*, vol. 17, no. 4, pp. 282–305, 2018.

[28] S. B. Martins, A. C. Telea, and A. X. Falcão, "Investigating the impact of supervoxel segmentation for unsupervised abnormal brain asymmetry detection," *Computerized Medical Imaging and Graphics*, vol. 85, p. 101770, 2020.

[29] J. E. Vargas-Muñoz, A. S. Chowdhury, E. B. Alexandre, F. L. Galvão, P. A. V. Miranda, and A. X. Falcão, "An iterative spanning forest framework for superpixel segmentation," *IEEE Transaction on Image Processing*, vol. 28, no. 7, pp. 3477–3489, 2019.

[30] J. R. Taylor, N. Williams, R. Cusack, T. Auer, M. A. Shafto, M. Dixon, L. K. Tyler, R. N. Henson *et al.*, "The cambridge centre for ageing and neuroscience (Cam-CAN) data repository: structural and functional mri, meg, and cognitive data from a cross-sectional adult lifespan sample," *Neuroimage*, vol. 144, pp. 262–269, 2017.

[31] S.-L. Liew and et al., "A large, open source dataset of stroke anatomical brain images and manual lesion segmentations," *Scientific Data*, vol. 5, p. 180011, 2018.

[32] A. X. Falcão, T. V. Spina, S. B. Martins, and R. Phellan, "Medical image segmentation using object shape models: A critical review on recent trends, and alternative directions," *Proc. of the Eccomas Thematic Conference on Computational Vision and Medical Image Processing (VipIMAGE)*, pp. 9–15, 2015.

[33] S. B. Martins, T. V. Spina, C. L. Yasuda, and A. X. Falcão, "A multi-object statistical atlas adaptive for deformable registration errors in anomalous medical image segmentation," in *SPIE Medical Imaging*, vol. 10133, 2017, pp. 691–698.

[34] S. B. Martins, A. X. Falcão, and A. C. Telea, "Combining registration errors and supervoxel classification for unsupervised brain anomaly detection," in *Biomedical Engineering Systems and Technologies*. Springer International Publishing, 2021, pp. 140–164.

[35] A. Z. Peixinho, S. B. Martins, J. E. Vargas, A. X. Falcão, J. F. Gomes, and C. T. N. Suzuki, "Diagnosis of human intestinal parasites by deep learning," in *Proc. of the Eccomas Thematic Conference on Computational Vision and Medical Image Processing (VipIMAGE)*, 2015, p. 107.

[36] T. V. Spina, S. B. Martins, and A. X. Falcão, "Interactive medical image segmentation by statistical seed models," in *Conference on Graphics, Patterns and Images (SIBGRAPI)*, 2016, pp. 273–280.

[37] S. B. Martins, G. Chiachia, and A. X. Falcão, "A fast and robust negative mining approach for enrollment in face recognition systems," in *Conference on Graphics, Patterns and Images (SIBGRAPI)*, 2017, pp. 201–208.

[38] J. Bragantini, S. B. Martins, C. Castelo-Fernandez, and A. X. Falcão, "Graph-based image segmentation using dynamic trees," in *Iberoamerican Congress on Pattern Recognition (CIARP)*, 2018, pp. 470–478.

[39] A. M. Sousa, S. B. Martins, A. X. Falcão, F. Reis, E. Bagatin, and K. Irion, "ALTIS: A fast and automatic lung and trachea CT-image segmentation method," *Medical Physics*, vol. 46, no. 11, pp. 4970–4982, 2019.